ELSEVIER

Contents lists available at ScienceDirect

Electrochimica Acta

journal homepage: www.journals.elsevier.com/electrochimica-acta





Comparison of carbon-nanofiber and carbon-nanotube as conductive additives in Si anodes for high-energy lithium-ion batteries

Jun Wei Yap, Tianyang Wang, Hanna Cho*, Jung-Hyun Kim*

Mechanical and Aerospace Engineering, The Ohio State University, Columbus, OH 43210, United States

ARTICLE INFO

Keywords: Li-ion batteries Si anodes Conducting additive Carbon nanotube Carbon nanofibers

ABSTRACT

This work presents a comprehensive analysis of the impact of carbon nanotubes (CNT) and carbon nanofibers (CNF) composition on the performance of nano-Si anodes in lithium-ion batteries. The nano-Si anode suffers from chemo-mechanical issues caused by its large volumetric change (e.g., 280%) during cycling. One of the promising solutions in electrode level is to establish a robust electronic conduction pathway in Si anodes by incorporating CNT and CNF with high aspect ratios. The objective of this work is to quantitatively measure the performance improvement achieved by CNT and CNF based on their compositions and analyze the improvement mechanism through electrochemical methods. The results indicate that substituting a portion of carbon black with CNT and CNF in a range of 1-10 wt% can enhance the capacity retention (from 44% to around 60%) and the fast-charging and fast-discharging capabilities. Electrochemical impedance spectroscopy (EIS) and distribution of relaxation times (DRT) analyses revealed that 5%-10% CNT and CNF conductors effectively suppressed contact impedances growths in Si anodes. In summary, our findings highlight the importance of precise control over the composition of CNT and CNF to achieve good electrode morphology and electrochemical properties for nano-Si anodes.

1. Introduction

Recent rapid development in electric vehicles has led to increasing demand for Li-ion batteries with high energy density. To address this demand, Si anodes has been suggested as an alternative to commonly used graphite anode because of their higher theoretical specific capacity of 4200 mAh/g, compared with 372 mAh/g of graphite anode [1,2]. However, fully lithiated Si (e.g., Li_{4.4}Si) can lead to a large volume expansion (> 300%), which leads to fracture of Si particle, loss of Si particles, and consequently solid electrolyte interface (SEI) degradation [3]. In addition, the repeated volumetric changes of Si resulted in mechanical stress and electrode delamination during repeated cycles [4]. These chemo-mechanical problems led to poor battery cycle life of Si anodes [5,6]. Recently, we reported that Si particles were cracked during de-lithiation and produced new SEI layer by using in-situ atomic force microscopy, which led to the cell impedance growth [7]. Si particle isolation was also observed during cycling battery cells [7], which contributed to a capacity fading. Beside these mechanical problems, Si anode itself suffers from slow reaction kinetics, low electronic conductivity and Li-ion diffusivity [8-10]. These problems compounded to present performance issue that hinders commercialization of pure Si anodes.

Various approaches have been explored in recent years to overcome the mechanical strain issues induced by Li-Si alloying and improve its cycle-life in battery cells. First, nanostructured Si materials have been developed actively because they can alleviate particle fractures and isolations during cycling process [11,12] For example, various Si nano-structures such as nano-particles, nano-wires [13], nano hollows [14], and nanotubes [15] has been demonstrated. Among them, Si nano-particles have been stood out due to its relatively simple processes and thereby low processing cost compared with other complex nanostructures.

It is also equally important to retain good electronic conduction pathway of Si nano-powders within anodes during cycling. To this end, carbon nanotube (CNT) and carbon nanofiber (CNF) are often used as conductive additives to supplement carbon black. The carbon black, spherical nano-powders, offers point-to-point contacts between Si particles [16]. In contrast, the one-dimensional CNT and/or CNF could provide line-to-line contacts between Si particles, which increase electroconductivity of the anode and improve the electrochemical

E-mail addresses: cho.867@osu.edu (H. Cho), kim.6776@osu.edu (J.-H. Kim).

^{*} Corresponding authors.

performance [16–18]. In addition, recent studies demonstrated that both CNT and CNF can partially subdue the detrimental effects of Si particle volume expansion by improving overall mechanical strength of Si anode via their 3D network structure within anodes [17–21]. Moreover, CNF could contribute to reducing tortuosity of electrolyte channels due to its dimensional impact on anode microstructure [22].

These improvement mechanisms can explain the benefits of adding CNT and CNF on improving the electrochemical performance (e.g., cyclability and rate capabilities) of Si anodes. However, there has been lack of systematic study that compares the effects of CNT and CNF on physical and electrochemical performances under the same anode processing and testing conditions. Quantifying the improvement brought about CNT and CNF compositions and characterizing the improvement mechanism will contribute to manufacturing high performance Si anodes. In this regard, we designed a systematic experiment that can compare the morphology and electrochemical properties of CNT and CNF-added Si anodes with various compositions. The results from this work will provide better guidance on selecting conductive additives for the optimization of nano Si anodes.

2. Experimental section

Si nano-sized powder (Nanostructured & Amorphous Materials, Inc) with an average particle size of 30–50 nm diameter was used as received. Si anode was prepared by mixing Si powder, 10 wt% lithiated polyacrylic acid (LiPAA), and carbon conductor (Super-P, MTI Corp.), at a weight ratio of 6:2:2. This electrode composition served as the control sample. The Super-P carbon black nanoparticles with average particle size of 40 nm, was partly replaced by multi-walled carbon nanotube (CNT, Sigma-Aldrich) or carbon nanofiber (CNF, Sigma-Aldrich). Here, both CNT and CNF were used as received, of which SEM images were shown in Fig. 1. The dimensions of CNT were 6 - 13 nm in diameter and 2.5 – 20 μ m in length, and the dimension of CNF were 100 nm in diameter and 20–200 μ m in length. Table 1 listed carbon combinations prepared and examined in this work.

The slurry was prepared by mixing nanosized Si powder and conductive carbons in a plastic bottle with zirconia grinding balls at a powder to ball wt. ratio of 15:1. In addition, the appropriate amount of water was added to reach the designated solid loading of 20%, followed

Table 1
List of samples and nomenclatures of various carbon compositions used for Si anodes in this work

Nomenclatures	Carbon Compositions
Baseline	100 wt% Super P
1% CNF	1 wt% of CNF / 99 wt% of Super-P
5% CNF	5 wt% of CNF / 95 wt% of Super-P
10% CNF	10 wt% of CNF / 90 wt% of Super-P
1% CNT	1 wt% of CNT / 99 wt% of Super-P
5% CNT	5 wt% of CNT / 95 wt% of Super-P
10% CNT	10 wt% of CNT / 90 wt% of Super-P

by mixing for two days using a roller mill (U.S. Stoneware, 801CVM). The resulting slurry was mixed with 10 wt% LiPAA binder at 2000 rpm for 10 min using a planetary mixer (Thinky, ARE310). The obtained slurry was coated on an electrodeposited copper foil (Sumitomo Metal Mining) using a doctor blade. After calendaring at 85 $^{\circ}$ C, all electrodes were vacuum dried at 80 $^{\circ}$ C overnight before moving into an Ar-filled glove box for cell fabrication.

Coin half cells (CR2032) were fabricated in the Ar-filled glovebox by using a Si anode, a piece of polypropylene separator (Celgard 2500), a lithium metal foil (Alfa Aesar), and a liquid electrolyte consisting of 1 M LiPF₆ in ethylene carbonate (EC) and diethyl carbonate (DEC) (EC:DEC = 1:1 vol. ratio) with 10% FEC. All coin cells were cycled by using a multichannel battery testing station (Arbin LBT system) at 25 °C in an environmental chamber. The cycling protocol was constant current (CC) - constant voltage (CV) charging (i.e., lithiation) and CC discharging (i. e., delithiation) in a voltage range of 1.5 - 0.005 V_{vs.Li} at C/20-rate for initial 3 cycles, followed by at C/10-rate for the remaining cycles. The fast charging and discharging capabilities were examined after three formation cycles at C/10-rate. EIS was measured (Gamry Interface 1010E) in a frequency range of 1 MHz - 0.1 Hz using AC amplitude of 3 mV. Before EIS measurement, cells were rested for 3 h at their fully discharged states. DRT analysis was also performed based on the EIS data [23]. Before the DRT analysis, Walburg diffusion tails from Nyquist plots were first removed.

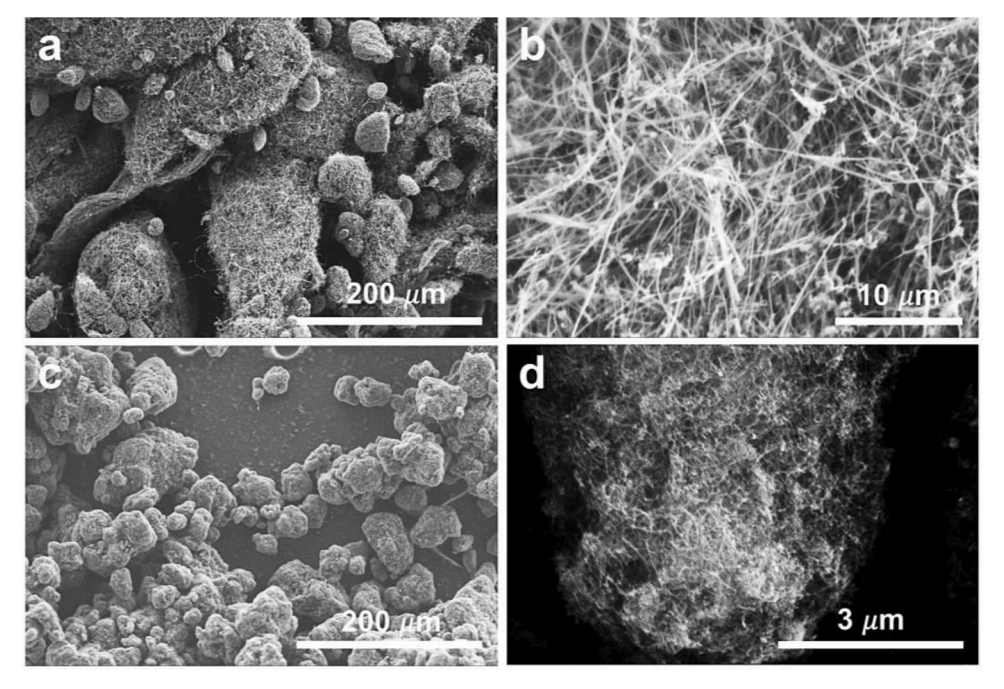


Fig. 1. SEM images of (a, b) carbon nanofibers (CNF) and (c, d) carbon nanotubes (CNT) used in this work.

3. Result and discussion

3.1. Effect of CNF and CNT on electrode morphology

Fig. 2 shows the surface morphology of fresh Si anodes with various CNT or CNF compositions. The baseline anode without CNT and CNF has revealed microcracks across the surface with approximately $100~\mu m$ dimensions that would be associated with LiPAA binder properties as reported earlier [24]. The 1% and 5% CNF added Si anodes (see, Fig. 2b and 2c) had reduced amounts of surficial cracks compared to the baseline anode (see, Fig. 2a) which can be attributed to the long-range (20–200 μm -length) network of CNF. However, larger amount of crack was observed from the 10% CNF electrode, indicating that there is adverse impact of excess CNF on the morphology of Si anode.

The addition of 1% CNT did not significantly change the morphology of the anode surface. However, an increase in CNT content to 5% and 10% led to a poor-quality coating. For example, they often exposed uncoated Cu foil surfaces as shown in Fig. 2f and 2g. The defects observed in CNT-added Si anodes may be related to the strong van der Waals force of CNTs, which can cause agglomeration of the CNT-Si composite [25], leading to an inhomogeneous coating layer. However, the exact defect mechanism and its correlation with hydrodynamics of aqueous solvents have yet to be fully explored and require further investigation in future studies. The result indicates that excess amounts of CNF (> 5 wt%) and CNT (> 1 wt%) negatively impact the homogeneity of the Si anodes.

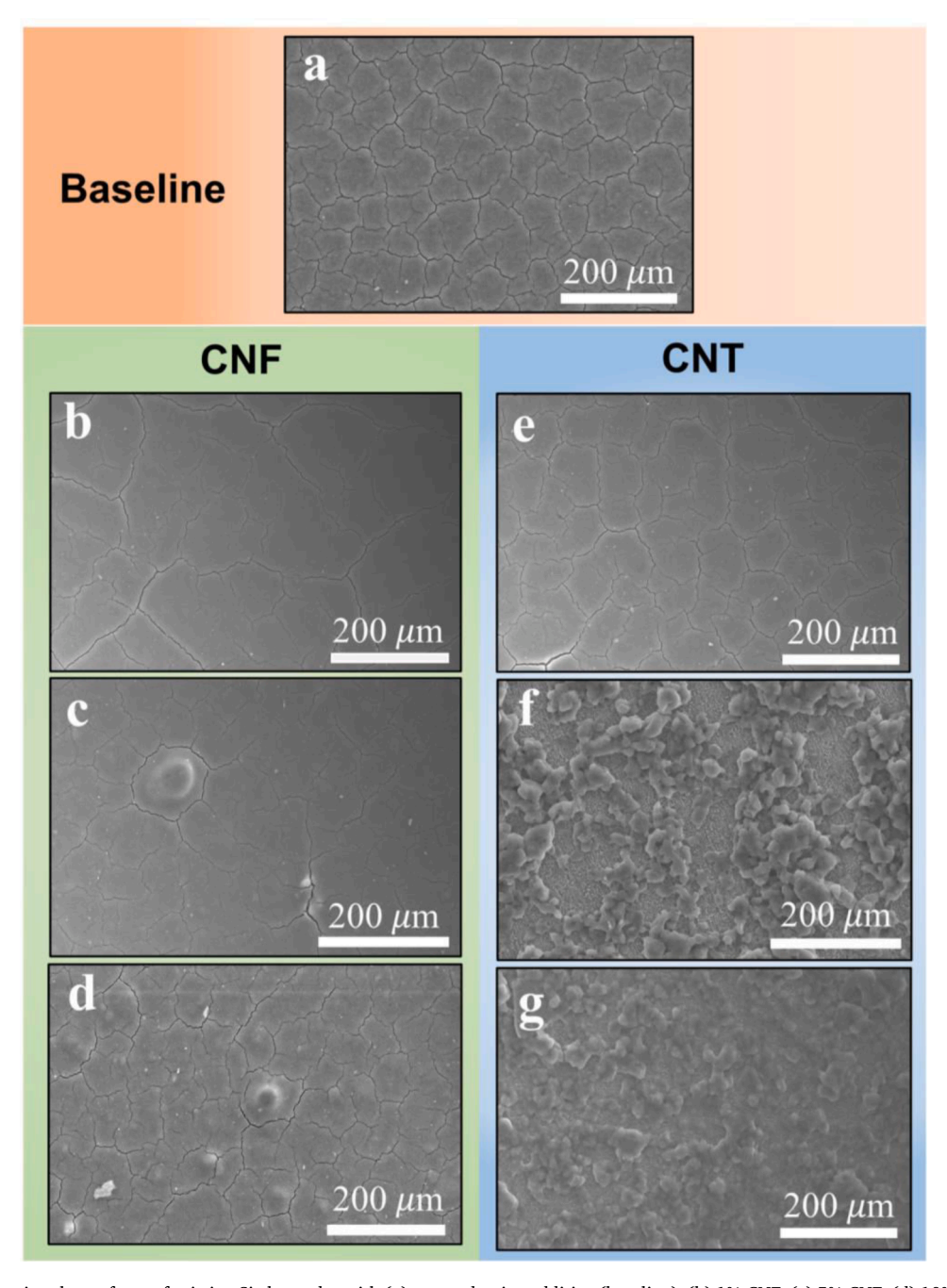


Fig. 2. SEM images showing the surfaces of pristine Si electrodes with (a) no conductive additive (baseline), (b) 1% CNF, (c) 5% CNF, (d) 10% CNF, (e) 1% CNT, (f) 5% CNT, and (g) 10% CNT.

3.2. Effect of CNF and CNT on cycle life

Fig. 3 compares the effect of CNF and CNT on the cycle life of the Si anodes in half-cells. Without CNF or CNT, the baseline anode delivered \sim 40% capacity retention at the 45th cycle. In contrast, improvement in the cycle life could be obtained by adding CNF or CNT. For example, increase in CNF content from 1% to 10% improved the normalized capacity retention values from \sim 44% to $\sim\!60\%$. It is worth noting that a considerable increase of \sim 19% in capacity retention was observed from the baseline to 5% CNF, while a marginal improvement of \sim 1.7% was observed from 5% CNF to 10% CNF. The results indicate that \sim 5% CNF will be the optimal carbon composition in terms of cycle life.

For CNT added Si anode (Fig. 3c and 3d), the addition of 1 wt% CNT did not offer a noticeable improvement on capacity retention. However, 5% CNT improved the capacity retention to $\sim 63\%$, followed by $\sim 55\%$ improvement from the 10% CNT. It is worthwhile to note that 5% and 10% CNT samples delivered improved cycle life despite their poor coating quality (see, Fig. 2f and 2g). This result suggests that Si anodes coated with 5% and 10% CNT still maintain good electrical contact.

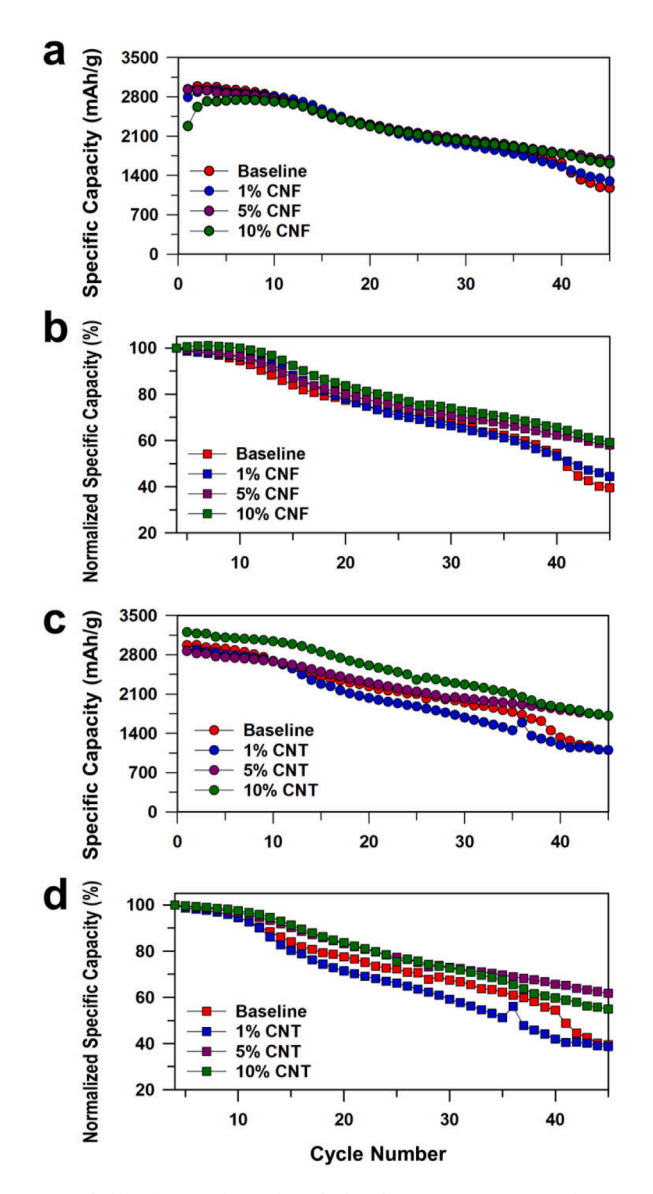


Fig. 3. Cycle life of Si anodes with (a, b) baseline (0%), 1%, 5%, and 10% CNF and (c, d) baseline (0%), 1%, 5%, and 10% CNT. All the half-cells were cycled at C/10-rate at 25 $^{\circ}$ C. (b, d) Normalization was performed based on the specific capacity at 4th cycle (i.e., after 3 formation cycles).

Overall, our data shows that CNT and CNF both improved capacity retentions of Si anodes.

The rapid capacity fading of the baseline Si anode in Fig. 3 is associated with physical degradation of Si and cell resistance growth during full-lithiation of Si up to $\text{Li}_{3.14}\text{Si}$. The stress from volume changes could induce particle crack, particle isolation, and capacity fading [7]. Employing the CNF or CNT will increase the carbon – Si contact areas due to their fiber/wire dimensions compared with that of simple carbon black (Super P). This enhanced carbon network can provide more stable electron conduction pathway within the anodes where severe mechanical evolution (e.g., crack or pulverization) of Si occurs, and therefore offers improved capacity retentions compared with the baseline anode.

The mechanical degradation of Si anodes can be partially alleviated by limiting the depth of charging (i.e., lithiation capacity). Using a capacity-limited cycling method, Si particles in anodes would experience reduced volumetric stress and consequently lesser mechanical degradation (e.g., crack, particle isolation, and particle pulverization). Fig. 4a and 4b show the capacity retentions and Coulombic efficiencies (CEs) of baseline, 10% CNT, and 10% CNF anodes in half-cells using the capacity-limited cycling protocol, where target charging (i.e., lithiation) capacity was limited to 1800 mAh/g. Under this condition, the cells delivered improved cycle life compared with the cycling at full-depth of lithiation (see, Fig. 3). The baseline anode showed capacity fading at 38th cycle and failed to reach the designated lithiation capacity of 1800 mAh/g at 41st cycle. In contrast, the 10% CNT anode did not experience the capacity fading until 43rd cycle, followed by slower degradation of discharge (i.e., delithiation) capacity and consequent failure at 51st cycle. The 10% CNF anode did not show the capacity fading until the 58th cycles but failed after that. This result implies that CNF is more effective at maintaining electronic conducting pathways in electrodes during the repeated volumetric changes of Si compared to CNT.

The voltage profiles and differential voltage (dQ/dV) profiles of the half-cells from capacity limited testing (Fig. 4) are presented in Fig. 5. At the 4th cycle, all the cells showed one major charging process at ~ 0.25 $V_{vs.Li}$ which was associated with a lithiation of Si to Li₂Si, followed by a minor charge process below ~ 0.2 $V_{vs.Li}$ which was associated with a

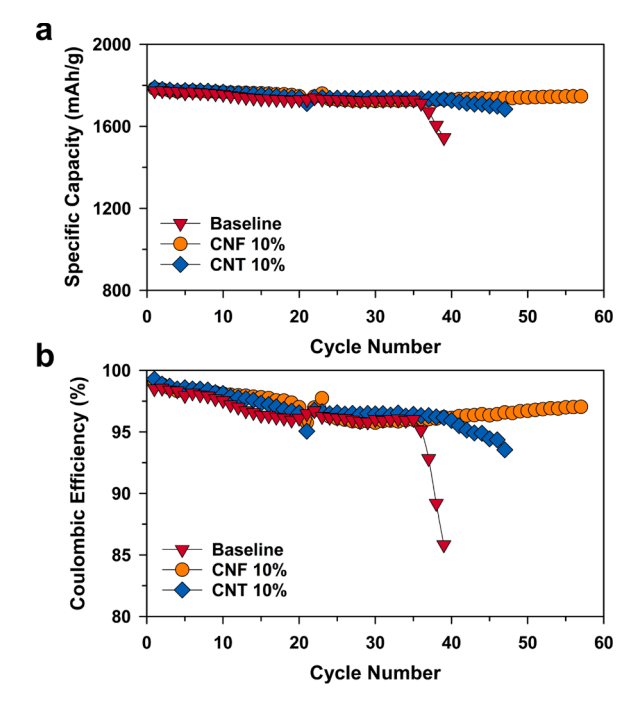


Fig. 4. (a) Cycle life and (b) Coulombic efficiency of baseline, 10% CNT, and 10% CNF anodes in half-cells at 25 $^{\circ}$ C, tested by using a capacity-limited cycling protocol (limited charging to 1800 mAh/g). The initial 3 formation cycles were not shown for simplicity.

J.W. Yap et al. Electrochimica Acta 446 (2023) 142108

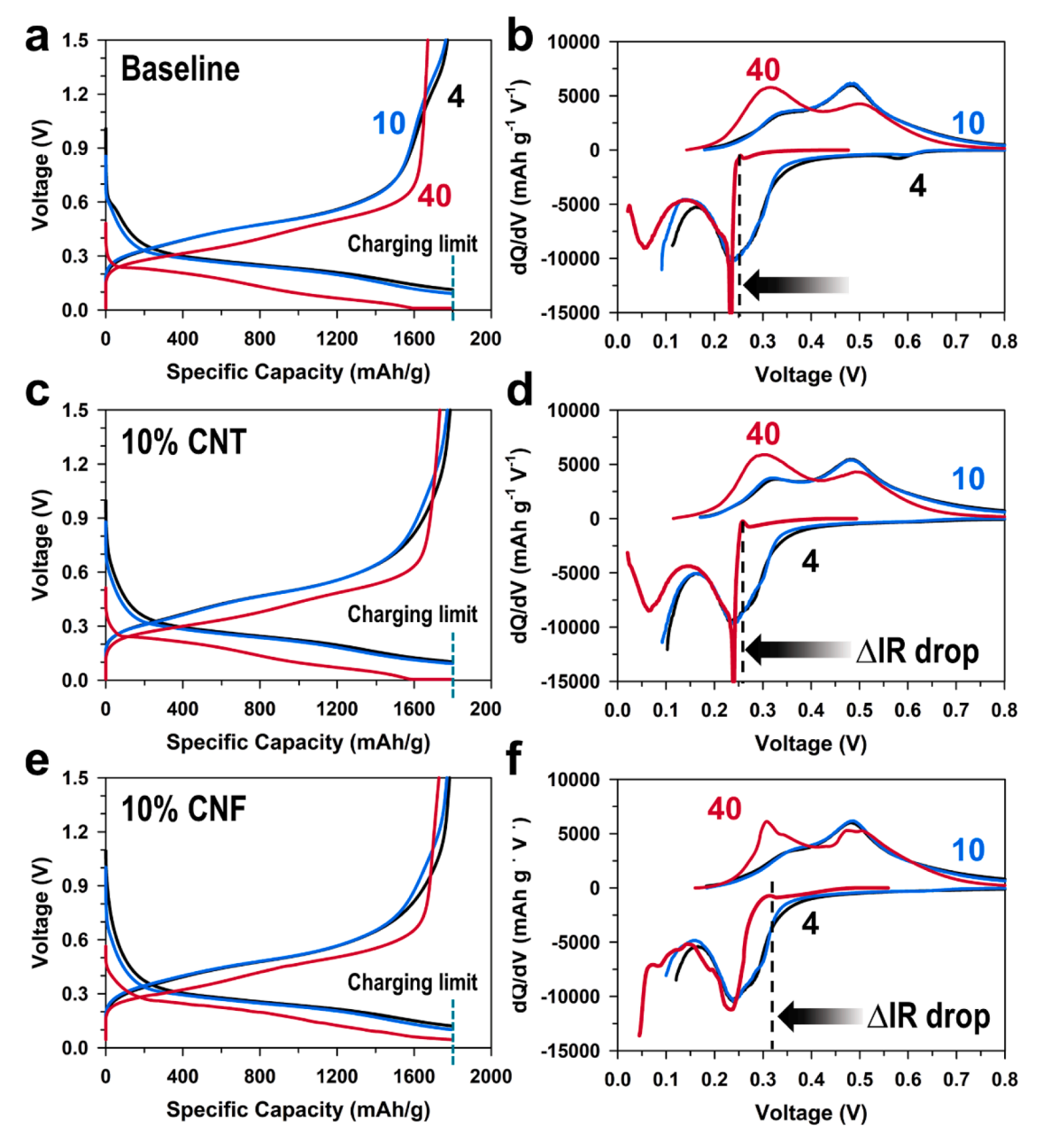


Fig. 5. Voltage and dQ/dV profiles at 4th, 10th, and 40th cycles of (a,b) baseline, (c,d) 10% CNT, (e, f) 10% CNF anodes in half-cells at 25 °C, tested by using a capacity-limited cycling protocol (limited charging to 1800 mAh/g).

lithiation of Li $_2$ Si to Li $_3$. $_5$ Si. At the 40th cycle, the first lithiation process at around 0.25 V $_{vs.Li}$ was suppressed with abrupt voltage drop ($\Delta I \bullet R$) at the beginning of the charging (i.e., lithiation) from the dQ/dV profiles (marked with arrow). Also, the decrease in the charge capacity at ~ 0.25 V $_{vs.Li}$ with cycle number can be in part caused by an active material's (Si) contact-loss during cycling. To deliver the net charge capacity of 1800 mAh/g, the aged Si anode should experience deep charging (x>2 in Li $_x$ Si at below 0.2 V $_{vs.Li}$) at 40th cycle, which unwantedly increased volumetric stress of Si [26]. This result confirms that the failure of the Si anodes stems from the gradual mechanical degradation of Si particles and increase in cell resistance.

Our results suggest that tailoring the carbon conductors enhances the electronic conduction network inside Si anodes. Specifically, adding 10% CNF is shown to provide a significant improvement in the conduction pathway as evidenced by (1) the lower $\Delta I \bullet R$ drop (i.e., lower electrode resistance), (2) maintaining good charge capacity at ~ 0.25 $V_{vs.Li}$ at 40th cycle, and (3) the improving overall cycle life.

3.3. Effect of CNF and CNT on rate capability

We further examined the effect of CNF and CNT addition on fast-charge and fast-discharge capabilities of the nano-Si anodes. Fig. 6a and 6b compare the fast-discharge (i.e., delithiation) capabilities of CNF and CNT added anodes, respectively. Baseline sample suffers from a rapid decrease in achievable capacity, reaching only $\sim\!300$ mAh/g at 7 C-rate. In contrast, fast-discharge capacity of Si anodes increased with increasing CNF or CNT contents from 1% to 10%. Both 10% CNF and 10% CNT delivered the best fast-discharge performance of around $\sim\!1650$ mAh/g at 7 C-rate. These results confirm that not only the long fiber length (e.g., $20-200~\mu\text{m}$) of CNF but also the intermediate lengths (e.g., $2.5-20~\mu\text{m}$) of CNT can improve the contact with Si nanoparticles and enhance electrical conduction within the anodes. Furthermore, the incorporation of CNF and CNT into the carbon network can help reduce particle isolation under severe volumetric stress during fast discharging, enabling a larger amount of Si active material to be utilized. At a given

J.W. Yap et al. Electrochimica Acta 446 (2023) 142108

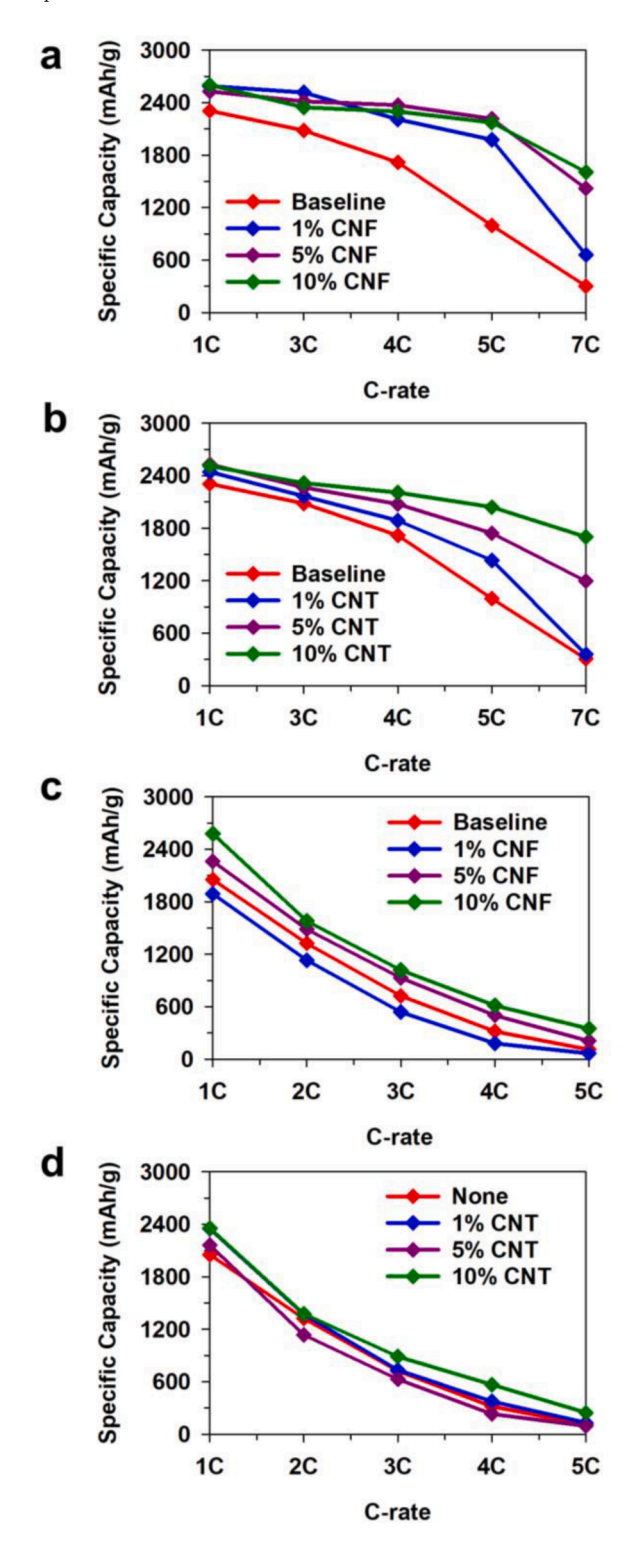


Fig. 6. Fast discharging (i.e., delithiation) capability of Si anodes with various (a) CNF and (b) CNT contents in half-cells. Fast charging (i.e., lithiation) capability of Si anodes with various (c) CNF and (d) CNT contents in half-cells; discharge capacities were plotted hear after the fast-charging.

content, CNF samples delivered slightly better fast-discharge capacity than CNT samples probably due to the relatively longer fiber length of CNF.

Figs. 6c and 6d compare the fast-charge (i.e., lithiation) capabilities of CNF and CNT added anodes, respectively. Here, it should be noted that the data plotted in Fig. 6c and 6d are discharge capacities obtained

after each fast-charging in a range of 1-5 C-rates. Similar to the fast-discharge test, baseline sample suffers from large capacity drop at high C-rates; e.g., $\sim\!100$ mAh/g at 5 C-rate. In contrast, the specific discharge capacities after the fast-charging increased with the amount of CNF, as shown in Fig. 6c. Compared to the CNF samples, Si anodes with 10 wt% CNT only provided a marginal capacity increase. In the range of 1-3 C-rates, Si anodes showed higher fast-charge capabilities with the order of 10% CNF >5% CNF >10% CNT, indicating the longer length of CNF providing better conductivity, hence better overall fast charging capability for Si anode.

The fast-charge capability of Si anodes was inferior to their fast-discharge capability. This trend agrees well with our earlier report [27], and can be explained by $\Delta I \bullet R$ drops of the cells at high C-rate. As shown in dQ/dV profiles (see, Fig 5), Li_xSi alloying (i.e., charging) could be incomplete during the constant-current (C.C.) charge process due to limited voltage windows down to 5 mV even at C/10-rate. The amount of $\Delta I \bullet R$ drops increase with higher C-rates, which in turn reduce the charge capacity significantly as well as the following discharge capacity. Although this incomplete charging issue can be partly alleviated by employing constant-voltage charging at the low cut-off voltage (e.g., 5 mV in this study), it unwantedly prolongs the charging time. In this work, we only used the C.C. charging process to compare intrinsic fast-charging capabilities between baseline and CNF/CNT added Si anodes.

3.4. Effect of CNF and CNT on cell impedances

Earlier section demonstrated that rate capability of Si anodes (particularly, fast-charge capability) was governed by the cell impedance. Therefore, we performed EIS characterization of various Si anodes [28]. Fig. 7 compares Nyquist plot of the baseline anode with those of CNF- or CNT-added Si anodes. The baseline anode suffers from significant impedance growth from the 4th cycle to 45th cycle. Compared to the baseline, anodes with CNF suppressed the growth of impedance from the 4th to 45th cycle with increasing CNF contents from 1 to 10%. Similar trend was observed from the CNT-added Si anodes. This EIS data agrees well with the electrochemical data presented in earlier sections.

The complex impedance behaviors of Si anodes were further analyzed by distribution of relaxation times (DRT) analysis to separate individual impedance responses appearing at different time domain (τ) from the Nyquist plots. Fig. 8 presents DRT plots obtained by processing Nyquist plots shown in Fig. 7. The DRT plots consisted of multiple peaks indexed by different colors. The high frequency ($\sim\!10^{3.5}$ Hz) peak (pink) corresponds to contact impedance from Si anode [29,30] while the two peaks (green and yellow) appearing in a range of 10^3 – 10^1 Hz correspond to impedance from SEIs on Li and Si [31,32]. The charge transfer peak that resides below 10^1 Hz is omitted from the DRT plots because of its unreliable value, which was caused by (i) artifact from Li SEI occurring at low frequency region which, in turn, (ii) distort Warburg type diffusion [28,33]. Such Li SEI driven errors at low frequency domain would negatively impact the accuracy of removing the diffusion tail from the Nyquist plot before the DRT analysis.

Fig. 9 compares the evolution of contact impedances determined by DRT analysis. The DRT data of the baseline Si anode showed that its contact impedance (pink) increased from 1.19 $\Omega \bullet mg$ (4th cycle) to 28.30 $\Omega \bullet mg$ (45th cycle). Such increase in contact impedance is an indicative of the electrical contact loss between Si particles or between Si and Cu-foil as a result of their chemo-mechanical degradation during cycling. Compared with the baseline anode, both CNF and CNT added Si anodes had significantly reduced contact impedance after 45th cycle. For example, the contact impedance values of CNF added Si anodes were 18.4 $\Omega \bullet mg$ (1% CNF), 2.7 $\Omega \bullet mg$ (5% CNF), and 9.4 $\Omega \bullet mg$ (10% CNF) at the 45th cycle. the contact impedance values of CNT added Si anodes were 19.9 $\Omega \bullet mg$ (1% CNT), 3.1 $\Omega \bullet mg$ (5% CNT), and 4.4 $\Omega \bullet mg$ (10% CNT) at the 45th cycle. In general, the 5% CNF and 5% CNT samples offered the lowest contact impedances, followed by the 10% CNF and

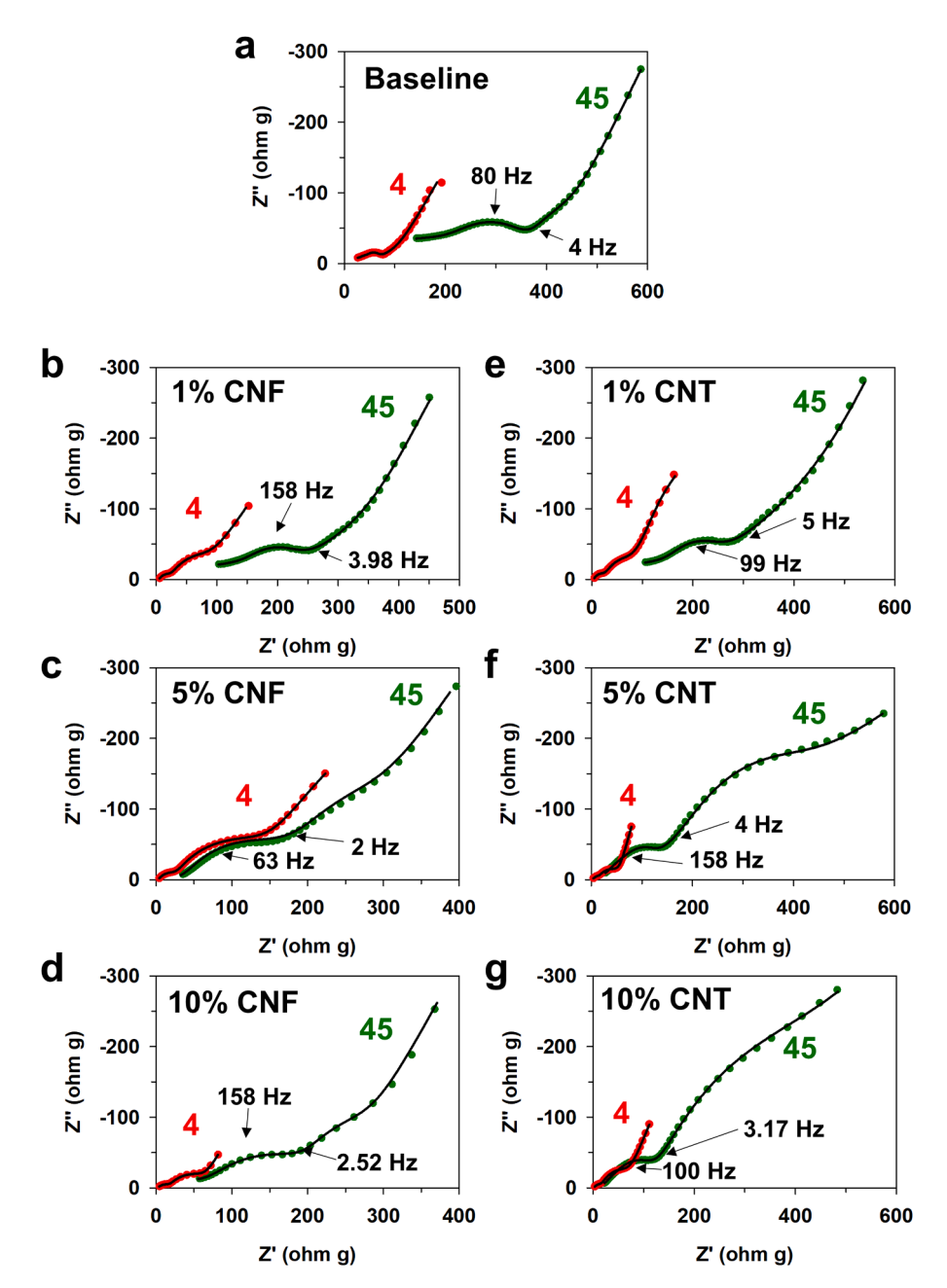


Fig. 7. Nyquist plots of Si anodes at 4th and 45th cycles in half-cells: (a) baseline, (b) 1% CNF, (c) 5% CNF, (d) 10% CNF, (e) 1% CNT, (f) 5% CNT, and (g) 10% CNT samples.

10% CNT. These DRT data unambiguously confirms the observation from Nyquist plots in Fig. 7, which showed significant decreases in contact impedances (at high frequency region of > 1000 Hz) for 5% - 10% CNF and CNF samples.

As for the SEI impedances (green and yellow) in the range of 10^3-10^1 Hz, there are no noticeable trend depending on the CNF or CNT contents. The changes in peak intensity are sporadic and not likely the result of CNF or CNT since their addition will not alter chemical properties/compositions of SEI layers on Si particles. This impedance data is in line with the cell performance data which showed that 5% and 10% CNF and CNT could lead to positive impacts on capacity retentions (see, Figs. 3 and 4) and rate capabilities (see, Fig. 6). The 1% CNT and CNF would not be enough to improve electrochemical performance of Si anodes.

4. Conclusions

Our systematic work demonstrated that by partially replacing carbon black with CNT and CNF conducting additives, the performance of nano-Si anodes can be significantly improved in terms of cycle life, rate capability, and cell impedance. The nano-Si anodes with 5%-10% CNF and CNT could improve capacity retentions due to the significant reduction in contact loss as evidenced by DRT analysis. Within the 5%-10% composition, CNF samples delivered improved fast-charge (between 1 C and 3 C-rates) and fast-discharge capability (between 1 C and 7 C-rate) compared to CNT samples. However, the inclusion of 1% CNF and 1% CNT did not result in a meaningful enhancement in the performance of nano-Si anodes. Our results demonstrated that well-controlled CNF compositions such as 5-10 wt% could achieve good electrode morphology and electrochemical properties of the nano-Si anodes. Although CNT also offered improved electrochemical

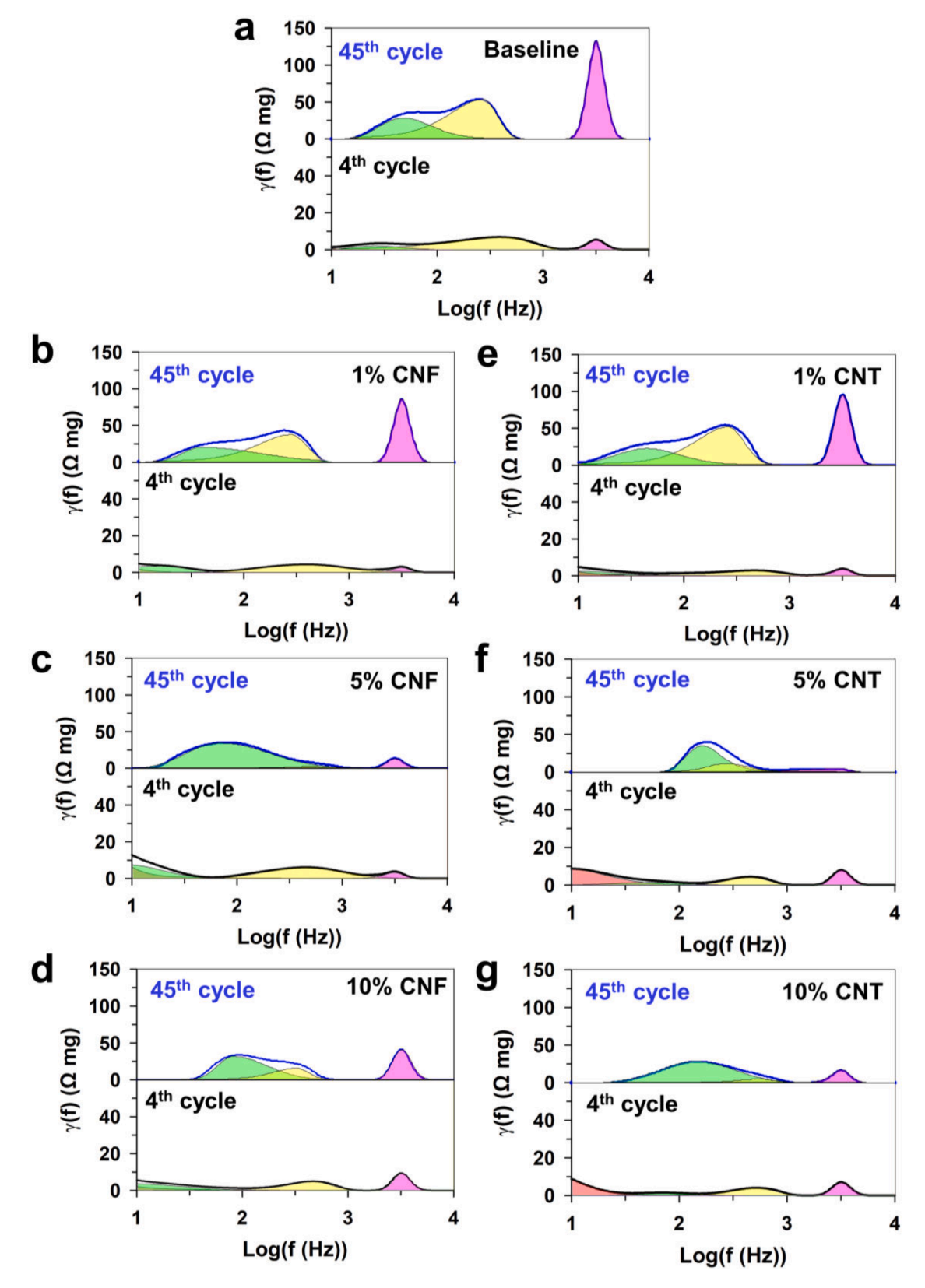
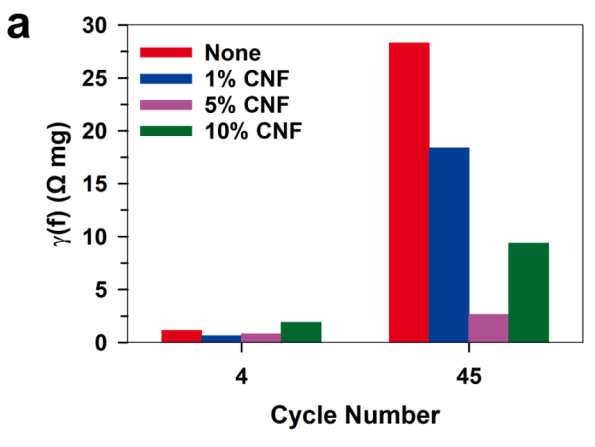


Fig. 8. DRT plots of Si anodes at 4th and 45th cycles in half-cells: (a) baseline, (b) 1% CNF, (c) 5% CNF, (d) 10% CNF, (e) 1% CNT, (f) 5% CNT, and (g) 10% CNT samples.

performances, 5 wt% and 10 wt% CNT caused noticeable deterioration in coating quality using our electrode processing methods. The outcomes of this comparative analysis between CNT and CNF can provide a valuable basis for the future optimization of nano-Si anodes, intended

for high-energy Li-ion battery applications.



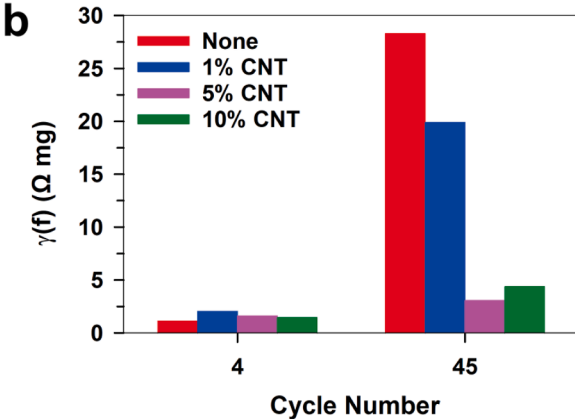


Fig. 9. Impedance growth for (a) CNF and (b) CNT added Si anodes comparing to bare Si anode (None). The values were determined by the DRT analysis.

CRediT authorship contribution statement

Jun Wei Yap: Conceptualization, Methodology, Investigation, Data curation, Writing – original draft. **Tianyang Wang:** Data curation, Writing – review & editing. **Hanna Cho:** Supervision, Conceptualization, Writing – review & editing. **Jung-Hyun Kim:** Supervision, Conceptualization, Writing – review & editing.

Declaration of Competing Interest

The authors declare that they have no known competing financial interests or personal relationships that could have appeared to influence the work reported in this paper.

Data availability

Data will be made available on request.

Acknowledgement

Characterization of this work was supported in part by The Ohio State University Institute for Materials Research.

References

- B.A. Boukamp, G.C. Lesh, R.A. Huggins, All-solid lithium electrodes with mixedconductor matrix, J. Electrochem. Soc. 128 (1981) 725–729, https://doi.org/ 10.1149/1.2127495.
- [2] D. Bresser, S. Passerini, B. Scrosati, Leveraging valuable synergies by combining alloying and conversion for lithium-ion anodes, Energy Environ. Sci. 9 (2016) 3348–3367, https://doi.org/10.1039/C6EE02346K.

- [3] L.Y. Beaulieu, T.D. Hatchard, A. Bonakdarpour, M.D. Fleischauer, J.R. Dahn, Reaction of Li with alloy thin films studied by in situ AFM, J. Electrochem. Soc. 150 (2003) A1457, https://doi.org/10.1149/1.1613668.
- [4] S.K. Soni, B.W. Sheldon, X. Xiao, A.F. Bower, M.W. Verbrugge, Diffusion mediated lithiation stresses in si thin film electrodes, J. Electrochem. Soc. 159 (2012) A1520–A1527, https://doi.org/10.1149/2.009209jes.
- [5] R. Kumar, A. Tokranov, B.W. Sheldon, X. Xiao, Z. Huang, C. Li, T. Mueller, Situ and operando investigations of failure mechanisms of the solid electrolyte interphase on silicon electrodes, ACS Energy Letters 1 (2016) 689, https://doi.org/10.1021/ acsenersylett.6b00284.
- [6] Y.H. Xu, G.P. Yin, P. Jian, Geometric and electronic studies of Li15Si4 for silicon anode, Electrochim. Acta 54 (2008), https://doi.org/10.1016/j. electrocta 2008 07 083
- [7] J. Liu, S.Y. Lee, J. Yoo, S. Kim, J.-.H. Kim, H. Cho, Real-time observation of mechanical evolution of micro-sized si anodes by in situ atomic force microscopy, ACS Materials Lett (2022) 840–846, https://doi.org/10.1021/ acsmaterialslett.2c00059.
- [8] M.T. McDowell, S.W. Lee, W.D. Nix, Y. Cui, 25th anniversary article: understanding the lithiation of silicon and other alloying anodes for lithium-ion batteries, Adv. Mater. 25 (2013) 4966–4985, https://doi.org/10.1002/adma.201301795.
- [9] Y.F. Gao, M. Zhou, Strong stress-enhanced diffusion in amorphous lithium alloy nanowire electrodes, J. Appl. Phys. 109 (2011), 014310, https://doi.org/10.1063/ 1.3530738.
- [10] M. Ko, S. Chae, J. Cho, Challenges in accommodating volume change of Si anodes for Li-Ion batteries, ChemElectroChem 2 (2015) 1645–1651, https://doi.org/ 10.1002/celc.201500254
- [11] M. Zhang, T. Zhang, Y. Ma, Y. Chen, Latest development of nanostructured Si/C materials for lithium anode studies and applications, Energy Storage Mater. 4 (2016) 1–14, https://doi.org/10.1016/j.ensm.2016.02.001.
- [12] Z. Ma, T. Li, Y.L. Huang, J. Liu, Y. Zhou, D. Xue, Critical silicon-anode size for averting lithiation-induced mechanical failure of lithium-ion batteries, RSC Adv. 3 (2013) 7398. https://doi.org/10.1039/c3ra41052h.
- [13] C.K. Chan, H. Peng, G. Liu, K. McIlwrath, X.F. Zhang, R.A. Huggins, Y. Cui, High-performance lithium battery anodes using silicon nanowires, Nat. Nanotechnol. 3 (2008) 31, https://doi.org/10.1038/nnano.2007.411.
- [14] H. Wu, G. Zheng, N. Liu, T.J. Carney, Y. Yang, Y. Cui, Engineering empty space between Si nanoparticles for lithium-ion battery anodes, Nano Lett. 12 (2012) 904–909, https://doi.org/10.1021/nl203967r.
- [15] T. Song, J. Xia, J.-H. Lee, D.H. Lee, M.-S. Kwon, J.-M. Choi, J. Wu, S.K. Doo, H. Chang, W.I. Park, D.S. Zang, H. Kim, Y. Huang, K.-C. Hwang, J.A. Rogers, U. Paik, Arrays of sealed silicon nanotubes as anodes for lithium ion batteries, Nano Lett. 10 (2010) 1710–1716. https://doi.org/10.1021/nl100086e.
- [16] Q. Lin, J.N. Harb, Implementation of a thick-film composite Li-ion microcathode using carbon nanotubes as the conductive filler, J. Electrochem. Soc. 151 (2004) A1115, https://doi.org/10.1149/1.1762878.
- [17] X. Fan, X. Zhang, G. Hu, B. Zhang, Z. He, Y. Li, J. Zheng, Single-walled carbon nanotube as conductive additive for SiO/C composite electrodes in pouch-type lithium-ion batteries, Ionics (Kiel) 26 (2020) 1721–1728, https://doi.org/10.1007/ s11581-019-03391-w.
- [18] X. Zhu, S.H. Choi, R. Tao, X. Jia, Y. Lu, Building high-rate silicon anodes based on hierarchical Si@C@CNT nanocomposite, J Alloys Compd 791 (2019) 1105–1113, https://doi.org/10.1016/j.jallcom.2019.03.354.
- [19] J. Guo, A. Sun, X. Chen, C. Wang, A. Manivannan, Cyclability study of silicon–carbon composite anodes for lithium-ion batteries using electrochemical impedance spectroscopy, Electrochim. Acta 56 (2011) 3981–3987, https://doi. org/10.1016/j.electacta.2011.02.014.
- [20] D. Mazouzi, D. Reyter, M. Gauthier, P. Moreau, D. Guyomard, L. Roué, B. Lestriez, Very high surface capacity observed using Si negative electrodes embedded in copper foam as 3D current collectors, Adv. Energy Mater. 4 (2014), 1301718, https://doi.org/10.1002/aenm.201301718.
- [21] L.Y. Lim, S. Fan, H.H. Hng, M.F. Toney, Operando X-ray studies of crystalline ge anodes with different conductive additives, J. Phys. Chem. C. 119 (2015) 22772–22777, https://doi.org/10.1021/acs.jpcc.5b05857.
- [22] Y. Kuang, C. Chen, D. Kirsch, L. Hu, Thick electrode batteries: principles, opportunities, and challenges, Adv. Energy Mater. 9 (2019), 1901457, https://doi. org/10.1002/aenm.201901457.
- [23] T.H. Wan, M. Saccoccio, C. Chen, F. Ciucci, Influence of the discretization methods on the distribution of relaxation times deconvolution: implementing radial basis functions with DRTtools, Electrochim. Acta 184 (2015) 483–499, https://doi.org/ 10.1016/j.electacta.2015.09.097.
- [24] L. Rao, X. Jiao, C.-Y. Yu, A. Schmidt, C. O'Meara, J. Seidt, J.R. Sayre, Y.M. Khalifa, J.-H. Kim, Multifunctional composite binder for thick high-voltage cathodes in lithium-ion batteries, ACS Appl. Mater. Interfaces. 14 (2022) 861–872, https://doi. org/10.1021/acsami_1019554
- [25] H. Yoon, H. Kim, P. Matteini, B. Hwang, Research trends on the dispersibility of carbon nanotube suspension with surfactants in their application as electrodes of batteries and proceedings of the patteries and process are process and process and process and process and process and process are process and process and process and process are process and proc
- [26] Q. Huang, M.J. Loveridge, R. Genieser, M.J. Lain, R. Bhagat, Electrochemical evaluation and phase-related impedance studies on silicon–few layer graphene (FLG) composite electrode systems, Sci. Rep. 8 (2018) 1386, https://doi.org/ 10.1038/s41598-018-19929-3.
- [27] K. Pan, F. Zou, M. Canova, Y. Zhu, J.-H. Kim, Systematic electrochemical characterizations of Si and SiO anodes for high-capacity Li-Ion batteries, J. Power Sources 413 (2019) 20–28, https://doi.org/10.1016/j.jpowsour.2018.12.010.

- [28] K. Pan, F. Zou, M. Canova, Y. Zhu, J.-H. Kim, Comprehensive electrochemical impedance spectroscopy study of Si-Based anodes using distribution of relaxation times analysis, J. Power Sources 479 (2020), 229083.
- [29] J. Illig, M. Ender, T. Chrobak, J.P. Schmidt, D. Klotz, E. Ivers-Tiffée, Separation of charge transfer and contact resistance in LiFePO 4 -cathodes by impedance modeling, J. Electrochem. Soc. 159 (2012) A952–A960, https://doi.org/10.1149/ 2.030207jes.
- [30] J. Illig, J.P. Schmidt, M. Weiss, A. Weber, E. Ivers-Tiffée, Understanding the impedance spectrum of 18650 LiFePO4-cells, J. Power Sources 239 (2013) 670–679, https://doi.org/10.1016/j.jpowsour.2012.12.020.
- [31] J. Illig, M. Ender, A. Weber, E. Ivers-Tiffée, Modeling graphite anodes with serial and transmission line models, J. Power Sources 282 (2015) 335–347, https://doi. org/10.1016/j.jpowsour.2015.02.038.
- [32] J.P. Schmidt, T. Chrobak, M. Ender, J. Illig, D. Klotz, E. Ivers-Tiffée, Studies on LiFePO4 as cathode material using impedance spectroscopy, J. Power Sources 196 (2011) 5342–5348, https://doi.org/10.1016/j.jpowsour.2010.09.121.
- [33] T.S. Ong, H. Yang, Symmetrical cell for electrochemical AC impedance studies of lithium intercalation into graphite, Electrochem. Solid-State Lett. 4 (2001) A89, https://doi.org/10.1149/1.1373377.